ACS NANO

www.acsnano.org

ARTICLE

Structural–Functional Integrated Graphene-Skinned Aramid Fibers for Electromagnetic Interference Shielding

Quanfen Guo,[▽] Huahui Tian,[▽] Yao Cheng,[▽] Shijun Wang, Zhaolong Li, He Hao, Jiayi Liu, Kun Jiao,* Xin Gao,* and Jin Zhang*

Cite This: https://doi.org/10.1021/acsnano.4c11782

Read Online

ACCESS | Metrics & More | Article Recommendations | Supporting Information

ABSTRACT: Structural–functional integrated polymer fibers with exciting properties are increasingly important for next-generation technologies. Herein, we report the structural–functional integrated graphene-skinned aramid fiber (GRAF) featuring high conductivity, high strength, and light weight, which is weaved for efficient electromagnetic interference (EMI) shielding. Graphene was self-assembled onto the surface of aramid fibers through a dip-coating strategy using an aramid polyanion (APA) as the binder and the etchant. The molecular dynamics (MD) simulation results show that the binding energy of the APA-modified aramid chain and graphene (1.3 J/m^2) is superior to that of the aramid chain and graphene (0.2 J/m^2). The APA has a higher surface energy (55.2 mJ/m^2) and can etch the fiber surface, forming grooves, which enables effective adsorption and self-assembly of graphene onto the fiber surface. The GRAF exhibits a high conductivity of 1062.04 ± 116.78 S/m, along with excellent strength (4.66 ± 0.16 GPa) and modulus (106.33 ± 8.21 GPa), outperforming most reported conductive composite fibers (e.g., natural fibers, polymer-based fibers, inorganic fibers, etc.). The weaved functional fabric using the structural–functional integrated GRAF shows an EMI shielding efficiency (SE) of up to 67.86 dB in the X-band and can rapidly heat up to 200 °C within 40 s at 12 V voltage. In addition, the GRAF fabric can maintain its electrical conductivity after a long-term washing, showing excellent washing resistance. This study demonstrates an effective method to fabricate structural–functional integrated materials and shows the promise of carbonene fibers for EMI shielding.

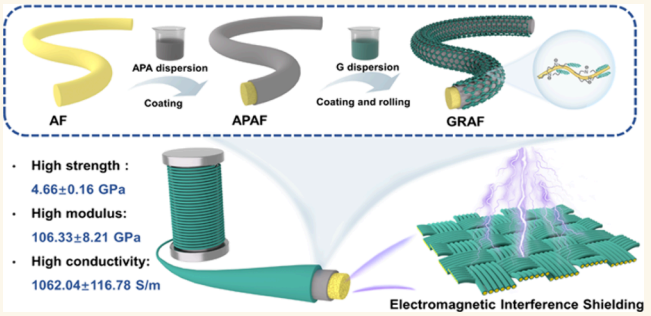

KEYWORDS: *structural–functional integration, graphene-skinned aramid fiber, aramid polyanion, dip-coating strategy, electromagnetic interference shielding*

INTRODUCTION

Aramid fiber is a typical high-performance polymer fiber, possessing notable advantages such as excellent mechanical properties, light weight, and high-temperature resistance,[1−3] showing great potential in impact protection.[4−6] However, the electrical insulation properties of aramid fibers pose limitations for other advanced applications such as electromagnetic protection, flexible electronic devices, and materials manufacturing. Therefore, imparting high electrical conductivity to high-strength aramid fibers will offer numerous opportunities to fabricate structural-functional integrated aramid fibers and develop next-generation technologies.

To enhance the electrical conductivity of aramid fibers, there are two main types of methods to consider: in situ polymerization doping and surface modification. Although the in situ polymerization doping method enhanced the fiber conductivity by fabricating a conductive filler network, it is hard to incorporate a large amount of conductive fillers into the aramid fibers due to the limitation of the spinning technology. Many studies show the enhanced electrical conductivity of aramid fibers by the surface modification.[7−9] For instance, gold nanoparticles are prepared on the Kevlar fiber surface using the electrochemical deposition method. The gold/Kevlar composite fiber can achieve a conductivity of over 100 S/m.[10] Similarly, a conductive Kevlar composite fiber was

Received: August 26, 2024
Revised: November 8, 2024
Accepted: November 20, 2024

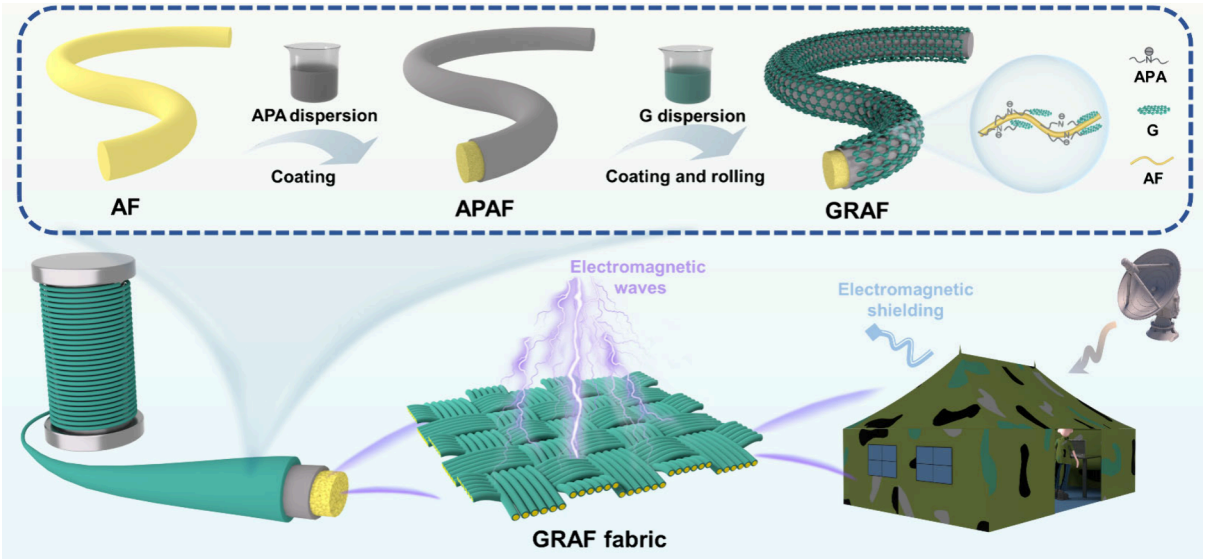

Figure 1. Schematic of the preparation process of GRAF and its application in electromagnetic protection. AF is the aramid fiber; APA is the aramid polyanion; APAF is the APA-modified aramid fiber; and GRAF is the graphene-skinned aramid fiber.

obtained by coating silver nanoparticles on the fiber surface using an intermediate poly(styrene-*block*-butadienstyrene) protective layer.[11] Recently, an MXene/Kevlar yarn was fabricated by using a continuous coating method by the weak van der Waals interaction between the MXene and the fiber. As-prepared MXene coated Kevlar yarn showed linear resistances of 5.3 Ω/cm and a strength of over 800 MPa.[12] These improvements drive the research field toward achieving high performance structural−functional integrated fibers. However, the electrical conductivities of as-prepared fibers still fall short of the anticipated level for practical applications, such as high-efficiency EMI shielding protection.[13] Further, the surface of the aramid fibers is smooth and chemically inert due to their high crystallinity. To achieve a strong combination with conductive materials, the above strategies typically employ a surface functional design between the conductive materials and aramid or the introduction of a polymer protective layer. As a result, aramid composite fibers often suffer from low mechanical strength[14] or high density/impurity.[15,16] The preparation of high performance structural−functional integrated aramid composite fibers with high strength, high conductivity, and light weight is still a great challenge.

Graphene is a two-dimensional material with excellent physical properties, including high carrier mobility, high electrical conductivity, high thermal conductivity, light weight, large specific surface area, and high mechanical strength.[17−19] Previous studies also demonstrated that graphene-based nanostructures showed excellent conductivity, electromagnetic interference shielding ability, and mechanical properties.[20−23] Therefore, graphene could be an ideal candidate for enhancing the electrical and mechanical properties of polymer composites. However, self-assembly of graphene onto smooth and chemically inert aramid fiber surface remains a great challenge due to the weak interaction between graphene and the polymer matrix.[24] Therefore, there is an urgent need to develop an efficient method for assembling graphene onto the fiber surface.

Inspired by the natural mussel binder, we developed an aramid polyanion (APA)-assisted strategy to self-assemble graphene onto the surface of heterocyclic aramid fibers (AF). APA not only promotes the degree of orientation and self-assemble ability of graphene on the fiber's surface but also imparts good washing stability to the fibers. The adsorption mechanism of APA was elucidated by a full-atom simulation. The conductivity of graphene-skinned aramid fiber (named GRAF hereafter) is 1062.04 ± 116.78 S/m, and the strength and modulus is 4.66 ± 0.16 GPa and 106.33 ± 8.21 GPa, respectively. The weaved functional fabric using the GRAF shows a rapid electrothermal response capability, which can be rapidly heated up to 200 °C within 40 s at 12 V voltage. More importantly, the GRAF fabric demonstrates an electromagnetic interference (EMI) shielding efficiency (SE) of up to 67.86 dB in the X-band with a very low graphene coating content (9.85 wt %), which outperforms most previously reported composite shielding materials. Our findings offer innovative strategies for synthesizing structural-functional integrated aramid fibers and fabrics with exceptional strength and conductivity.

RESULTS AND DISCUSSION

Preparation and Structural Characterization of GRAF.

The GRAF was prepared using an APA-assisted two-step coating strategy (Figure 1). The APA was synthesized via the deprotonation of the aramid polymer (Figure S1) using potassium hydroxide (KOH) solution (Figure S2) and then coated onto the fiber surface. The APA has high surface energy and can etch the AF surface forming grooves, which enables effective adsorption of graphene. With APA as the intermediate binding layer, the graphene was then self-assembled onto the fiber surface through the dip-coating process. Incorporating APA into the interface layer as an interface binder showed the following advantages: (1) The APA-modified aramid fiber (named APAF) exhibits a higher surface roughness than AF due to the etching effect of APA, which is beneficial to the self-assembly of graphene; (2) APA with a higher surface energy compared to aramid fibers enabled stronger adsorption between graphene and the fibers; (3) The APA mechanically locked with graphene, which significantly enhanced the stability of graphene coating; (4) APA is compatible with the aramid system without introducing any impurities. Subse-

https://doi.org/10.1021/acsnano.4c11782
ACS Nano XXXX, XXX, XXX−XXX

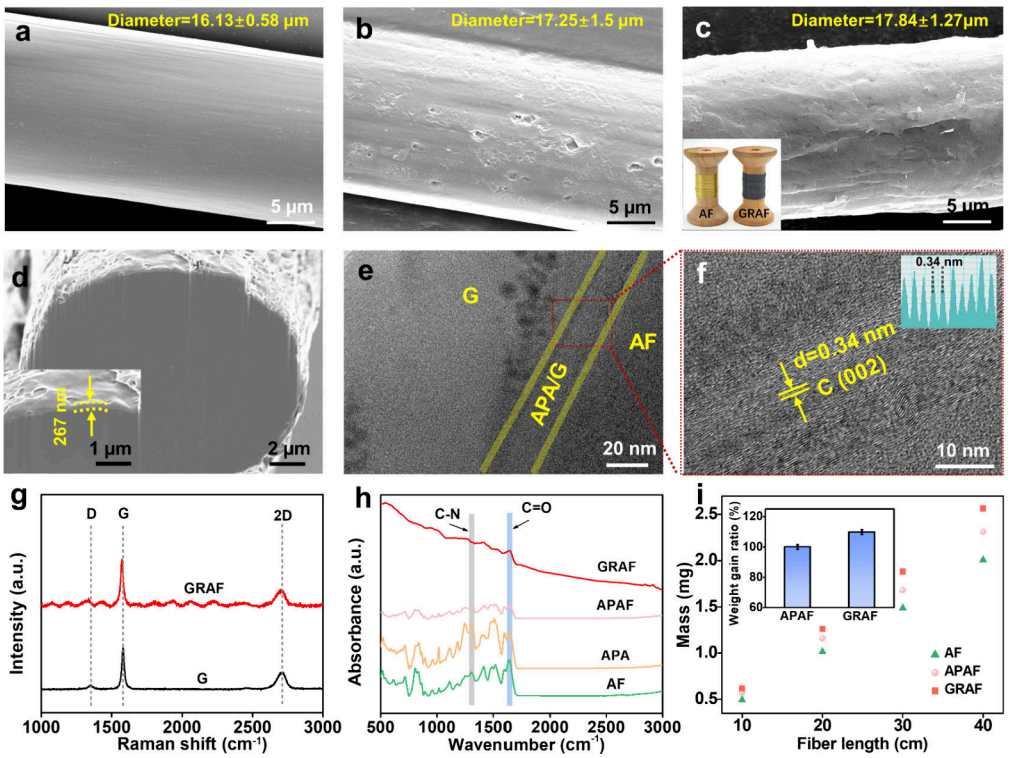

Figure 2. Characterization of GRAF. SEM images of (a) AF, (b) APAF, and (c) GRAF. The left insets in (c) are the photographs of AF and GRAF. (d) SEM images of the axial cross-section of GRAF. (e, f) TEM images of the axial cross-section of GRAF. (g) Raman spectra of graphene powder and GRAF. (h) FTIR spectra of AF, APA, APAF, and GRAF. (i) Weight gain ratio of APAF and GRAF after coating.

quently, conductive GRAF was fabricated via a series of straightforward procedures including drying (100 °C, 10 min), washing, and rolling. The GRAF exhibits exceptional mechanical and electrical properties, rendering it a highly versatile structural−functional integrated fiber. The woven fabric exhibits excellent electromagnetic shielding properties and electric heating capabilities, making it highly promising for applications in electromagnetic shielding tents, deicing protective skin, and other related fields.

The structures and properties of graphene are characterized as key factors affecting the electrical conductivity of the fibers. To investigate the conductivity of graphene, a glossy and compact graphene film (areal density is 10 g/m^2) was fabricated through vacuum filtration, showing a conductivity of ∼30 000 S/m. The graphene powder was also compressed into sheets to evaluate its electrical conductivity (6590 S/m, Figure S3a). The X-ray photoelectron spectroscopy (XPS) spectra showed a high C/O atomic ratio of 26.39 (Figure S3b), indicating the high quality of the graphene sheets.[25] The graphene nanosheets were further characterized by transmission electron microscopy (TEM), showing a thickness of 4−5 layers (Figure S3c). The average size of individual graphene nanosheets was around 3 μm (Figure S4a,b). To investigate how the concentration of graphene dispersion affects the GRAF structure, dispersions with different concentrations of graphene (1, 2, and 4 mg/g) were prepared. Using these graphene dispersions, we obtained different graphene-coated fibers (named as GRAF$_1$, GRAF$_2$, and GRAF$_4$). Using a low-concentration graphene dispersion (1 mg/g), the as-prepared GRAF surface showed a lower coverage of graphene (Figure S5a,d). When the concentration of graphene was increased to 2 mg/g, the AF was completely covered by the graphene nanosheets (Figure S5b,e). However, when the concentration of graphene dispersion is higher than the threshold (4 mg/g, GRAF$_4$), the fiber bundles were adhered to each other by excess graphene nanosheets (Figure S5c,f). Therefore, the optimal concentration of the graphene dispersion was 2 mg/g for GRAF preparation.

The morphologies of AF, APAF, and GRAF were characterized by using scanning electron microscopy (SEM). Compared with the smooth surface of AF (Figure 2a), the surface of APAF exhibited more grooves due to the etching effect of APA (Figure 2b). After graphene coating, the GRAF surface showed no significant groove, indicating compact contact between the graphene coating layer and the fibers (Figure 2c). The AF changed from a yellow color to black (insert of Figure 2c). The diameter of AF, APAF, and GRAF gradually increased from 16.13 ± 0.58 μm to 17.25 ± 1.5 μm and finally to 17.84 ± 1.27 μm (Figure S6). The axial cross-sectional SEM image showed that graphene was tightly and uniformly wrapped around the fiber surface, with a thickness of 267 nm (Figure 2d).

The microstructure of GRAF was further characterized by TEM. The left and right sides of the red dashed box in Figure 2e represent the graphene and AF matrix, respectively. The diffusion zone of APA and graphene was highlighted by the yellow lines. The zoomed-in image of the diffusion zone (Figure 2f) reveals that the APA induced the alignment of graphene nanosheets along the axial-direction of the fiber. Such orientation is conducive to enhancing the electrical conductivity of fibers.[26,27] Moreover, this well-defined orientation provides strong evidence for a strong interaction between graphene and APA. The Raman spectra of the GRAF demonstrated typical peaks of graphene (Figure 2g), indicating the successful self-assembly of graphene on the fiber surface. Moreover, the G-peak (1580 cm^{-1}) of graphene showed a

https://doi.org/10.1021/acsnano.4c11782
ACS Nano XXXX, XXX, XXX−XXX

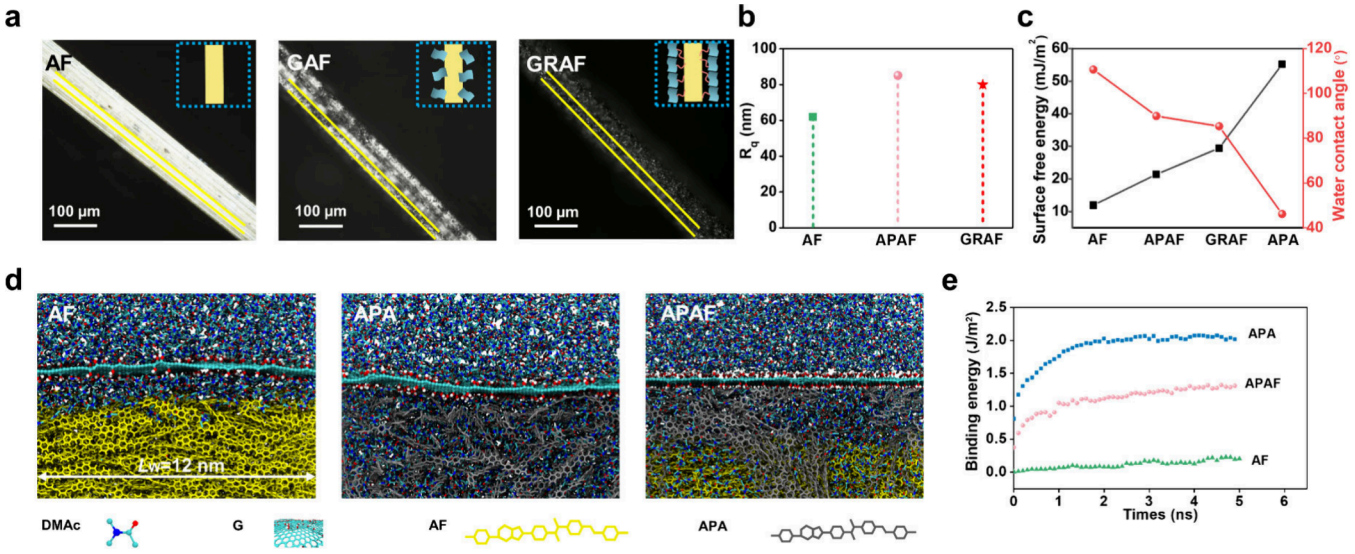

Figure 3. The working mechanism of the APA binder layer. (a) OM images of AF, GAF, and GRAF. (b) Roughness of AF, APAF, and GRAF. (c) Surface free energy and water contact angle of AF, APAF, GRAF, and APA. (d) Molecular dynamics simulation of the adsorption between AF, APA, and APAF sequentially with graphene. (e) Binding energies of AF chains and graphene (green dots), APAF chains and graphene (pink dots), APA chains and graphene (blue dots).

redshift after coating on the aramid fibers, which could be attributed to the stress and band structure change induced by the adsorption of APA.[28] The Fourier transform infrared (FTIR) spectra of the fibers are presented in Figure 2h and Figure S7. In comparison to the peaks observed at 1636 cm^{-1} for C═O and 1301 cm^{-1} for C−N in AF,[29,30] both peaks exhibit a blueshift in APA and APAF, resulting from the breaking of the hydrogen bond, which indicated the deprotonation of APA.

The graphene content on the surface of GRAF was determined by weighing fibers with different lengths. Figure 2i shows the weight percentage of graphene coating on the GRAF is 9.85 ± 1.61 wt %. This finding is consistent with the graphene content measured by the thermal gravimetric analyzer (9.50 wt %) as shown in Figure S8.

The self-assembly of graphene on the fiber surface was further observed using an optical microscope (OM) (Figure 3a). The AF exhibits a bright white appearance. Subsequently, the graphene-coated aramid fibers (GAF) without the APA interlayer showed a decrease in brightness. Notably, the GRAF exhibits a distinct black appearance, indicating a substantial graphene coating on the fiber surface. This observation further validates the efficacy of APA for facilitating graphene adsorption onto the fiber surface. The surface morphologies of AF, APAF, and GRAF were characterized using atomic force microscopy (AFM). As depicted in Figure 3b and Figure S9, the root-mean-square (RMS) roughness (R_q) values for AF, APAF, and GRAF are 62, 85.1, and 80 nm, respectively. The surface roughness of the fiber increased after APA modification, which results in a larger contact area thereby promoting stronger interface interaction between the fibers and graphene.[31] The water contact angle and surface energy of the fibers were presented in Figure 3c and Figure S10. APA had the highest surface energy (55.2 mJ/m^2), which was attributed to hydrogen bond disruption at the amide bond site. After incorporating APA, the surface energy of AF increased from 11.95 to 21.23 mJ/m^2, accompanied by a decrease in the water contact angle from 110.65° to 89.9°. Incorporating APA effectively enhanced the surface energy of the fiber. In general, the augmentation of surface energy can enhance the wettability of the matrix fibers and promote interface compatibility between the fiber and graphene, thereby facilitating graphene adsorption onto the fibers.[32,33] The GRAF showed a surface free energy of 29.47 mJ/m^2 and a water contact angle of 85.30°. The ζ potential results also provide additional evidence supporting the absence of any electrostatic attraction between graphene and APA, since both are negatively charged (Figure S11).

Further, molecular dynamics (MD) simulation was employed to investigate the adsorption behavior of graphene on the surfaces of AF and APA (Figure 3d and Figure S12). The MD simulation results revealed that dimethylacetamide (DMAc) solvent molecules used for graphene dispersions were situated between the graphene and the AF, hindering their effective contact. Therefore, the direct coating of graphene onto the AF surface is very challenging. By contrast, the APA molecular chain within the DMAc solvent enabled complete contact with graphene without any noticeable DMAC layer. This implies that compared to AF, the APA structure can more easily achieve efficient contact with dispersed graphene in the DMAc solvent. Figure 3d shows the adsorption behavior of graphene on the AF surface after incorporation of APA. The APA molecular chain exhibited not only entanglement with AF but also integration with graphene. Consequently, during the coating process, APA worked as the binder, establishing a crucial link between graphene and AF, thus facilitating the adhesion between the graphene and the AF surface. To further understand the interaction between graphene and fibers, we calculated the binding energies of the AF chain, the APAF chain, and the APA chain with graphene (Figure 3e). The APA chain exhibited a stronger binding energy with graphene compared with the AF chain. When the APA is coated on the surface of the AF, the binding energy of the APAF chain and graphene (1.3 J/m^2) surpasses that of the AF chain and graphene (0.2 J/m^2). Meanwhile, the binding energy between the APA and the AF chain is about 0.3 J/m^2 (Figure S13), which is also higher than those of the AF chain and the graphene. These findings align well with previous experimental

https://doi.org/10.1021/acsnano.4c11782
ACS Nano XXXX, XXX, XXX−XXX

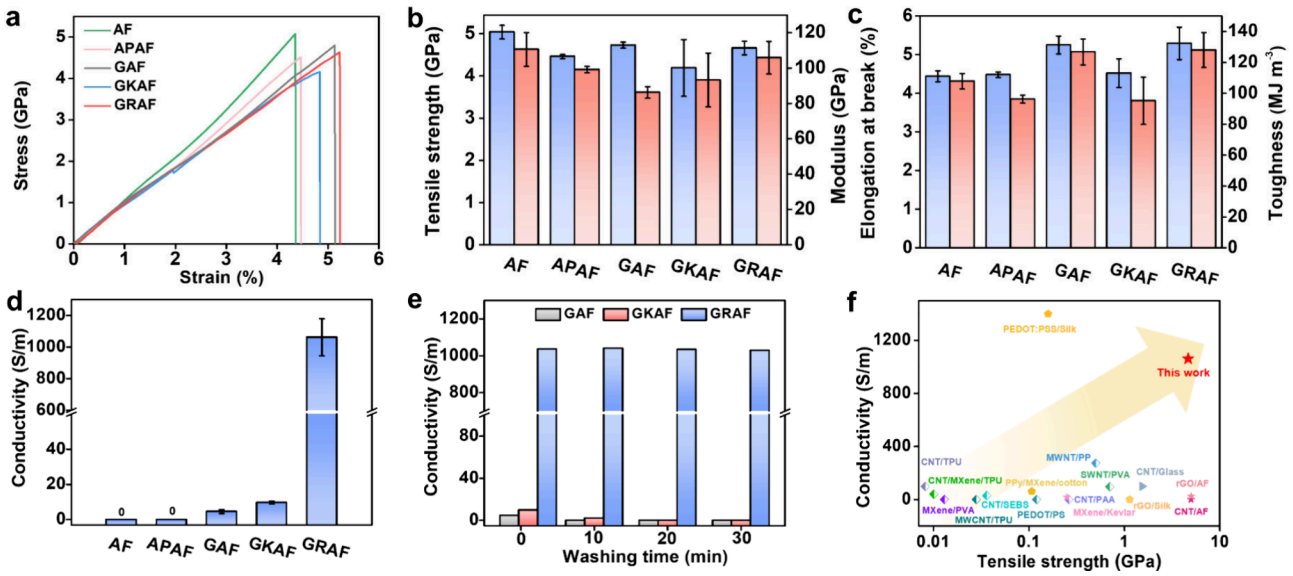

Figure 4. Mechanical and electrical properties of designed GRAF. (a) Stress−strain curves of different fibers. (b) Comparison of the tensile strength and Young's modulus of different fibers. (c) Comparison of the elongation at break and toughness of different fibers. (d) Electrical conductivity curves of different fibers. (e) Comparison of electrical conductivity of fibers at different washing times. (f) Comparison of electrical conductivity and tensile strength of different conductive composite fibers and our prepared fiber.

results, suggesting that incorporating APA facilitates the self-assembly of graphene on the fiber surface.

Mechanical and Electrical Properties of Designed GRAF. The mechanical property is a crucial parameter for fibers with integrated structure−function. We investigated the mechanical properties of the fibers through monofilament testing. For comparison, GAF and graphene-coated KOH modified aramid fiber (GKAF) were prepared using the same coating method, and their morphology is depicted in Figure S14. Figure 4a illustrates the stress−strain curves of the fibers. By comparing the tensile strength and modulus among different fibers (Figure 4b), it is evident that the fibers modified by APA, G, or KOH exhibited a decline in these properties when compared to AF. Specifically, APAF exhibited a tensile strength and modulus of 4.46 ± 0.05 GPa and 99.15 ± 1.76 GPa, respectively. This decrease can be attributed to the surface etching and diameter increase by the modification of an APA polymerization solution. Moreover, graphene self-assembly led to a notable enhancement in both tensile strength (4.66 ± 0.16 GPa) and modulus (106.33 ± 8.21 GPa) for GRAF compared to the APAF, corresponding to increases of 4.48% and 7.24%, respectively. Notably, the APA/G bonded interface layer formed through $\pi-\pi$ interactions and mechanical interlocking between APA and graphene tightly adhered to the surface of the AF. This interface layer facilitates efficient load transfer during continuous loading and aids in stress dissipation during dissociation, thereby enhancing the strength of the GRAF.[34,35] Moreover, the increased modulus resulted from strong adsorption and induced orientation of APA on graphene, facilitating a dense packing arrangement of numerous graphene nanosheets on the surface of the fiber.[36]

Figure 4c shows that the elongation at break of all fibers modified with APA, G, or KOH is increased. Among them, the GRAF exhibits the highest elongation at a break of 5.29 ± 0.42%, which is 19.14% and 18.08% higher than that of AF and APAF, respectively. This is mainly due to the strong interaction between the APA and the graphene layer during stretching, which can bond the graphene layer and provide longer sliding distance of the graphene sheet before breaking.[37] It is well-known that fiber toughness is determined by a combination of elongation and tensile strength, and the area under the stress−strain curve can be used to express the material's toughness.[38] The calculations showed that the toughness of GRAF is 128.02 ± 9.96 MJ m^{-3}, which is 18.69% and 33.08% higher than that of AF and APAF, respectively.

Figure 4d shows the electrical conductivities of different fibers. The conductivities of GAF, GKAF, and GRAF were 4.60 ± 1.04, 9.69 ± 0.79, and 1062.04 ± 116.78 S/m, respectively. To assess the stability of the graphene coating on the fiber surface, we conducted a simulated washing process by immersing the fiber in water and subjecting it to stirring at a speed of 5000 rpm for different durations (Figure S15a). The GAF showed electrical insulation properties after 10 min of washing. The GKAF is electrically insulating after 20 min of washing. For GRAF, the electrical conductivity remained stable even after 30 min of washing (Figure 4e). Figure S15b revealed that the GRAF retained a dense graphene layer on its surface after 30 min of washing. We performed the tape testing to further characterize the structural stability of the GRAF fibers. There was no visible graphene on the tape, and the conductivity of the fiber remained unchanged even after multiple taping-stripping (Figure S16a−d). These results indicated that the surface graphene coating was stabilized by the strong interaction between APA and graphene.

Furthermore, the mechanical properties and electrical conductivity of GRAF were compared with those of glass fibers, cotton fibers, silk fibers, aramid fibers, and other polymer fibers modified with carbonene materials, MXene, or conductive polymers (Figure 4f, Table S1).[39−54] The GRAF exhibited both higher electrical conductivity and higher tensile strength, making it a structural-functional integrated fiber with outstanding mechanical and electrical characteristics. The findings depicted in Figure S17 and Table S2 provided further substantiation for this conclusion. The outstanding performance of GRAF can be attributed to the following factors. First,

https://doi.org/10.1021/acsnano.4c11782
ACS Nano XXXX, XXX, XXX−XXX

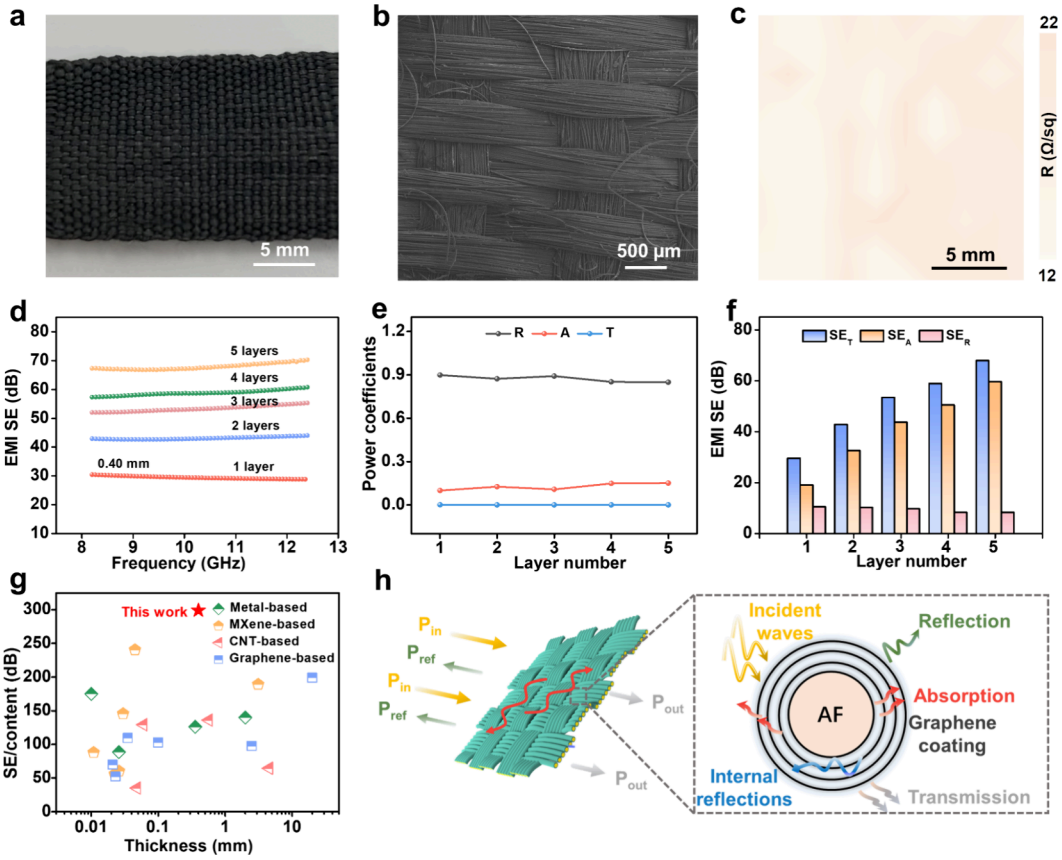

Figure 5. GRAF fabric and its electromagnetic interference shielding properties. (a) Digital photo, (b) SEM image, and (c) sheet resistance mapping of GRAF fabrics. (d) EMI shielding performance of the GRAF fabrics with various layers in the frequency range of 8.2−12.4 GHz. (e) Power coefficients *A*, *R*, and *T* of GRAF fabrics. (f) SE_T, SE_R, and SE_A values of GRAF fabrics with different layers. (g) Comparison of EMI SE/content of GRAF fabrics with the reported EMI shielding materials of different thicknesses. (h) EMI shielding mechanism of GRAF fabrics.

incorporating APAs as the binder resulted in a higher content of graphene (9.85 wt %) in the composite fibers than that of previous results in the literature. Second, we selected graphene with a highly crystalline structure and large-area sheets for achieving a high electrical conductivity of the composite fiber. Third, the excellent mechanical properties of the aramid fiber can be maintained using the mild coating method. Consequently, GRAF showed promise for applications in high-strength protection and electromagnetic shielding.

Electric Heating and EMI Properties of the GRAF Fabrics. We wove the high strength and high conductivity GRAF into fabrics for fast electric heating and efficient electromagnetic interference shielding. Figure 5a and Figure 5b are the digital photographs and SEM images of GRAF fabrics, respectively. The fabric resistance mapping in Figure 5c demonstrated a good uniformity of the graphene coating, exhibiting an average value of 17.03 ± 3.08 Ω/sq across a 1.75 cm × 1.75 cm area. The resistance of the fabric remained almost unchanged and maintained its original shape under different combustion times (Figure S18), ensuring its stability in practical applications. In addition, the washing resistance of the GRAF fabric was evaluated by the washing test. The GRAF fabric can maintain its electrical conductivity after a 120 min washing at a speed of 800 rpm (equivalent to 6 standard tests, Figure S19).

We first investigated the electric heating properties of the GRAF fabrics. Figure S20a illustrates the typical surface temperature variation of the GRAF fabrics during a single heating−cooling cycle under different applied voltages (6, 8, 10, and 12 V). It can be observed that a stable surface temperature was rapidly achieved within 40 s for all voltage levels, indicating the highly efficient electric heating characteristic of our prepared GRAF fabrics. Surprisingly, increasing the input voltage from 6 to 12 V resulted in a wide electrothermal temperature range (45−200 °C) for GRAF fabrics (Figure S20a,b). Figure S20c presents an infrared image of the GRAF fabrics electrothermal device with a bent angle of 180° under 12 V voltage, demonstrating its uniform temperature distribution. Moreover, due to excellent joule heating capabilities, the GRAF fabrics prove effective in combating frost or ice in extremely cold weather conditions.[55,56] The GRAF fabrics exhibit excellent electrical conductivity, making them suitable for use as a conductor in circuits to illuminate a lamp at 4.5 V. The lamp maintained its original brightness even when the fabric was subjected to bending or twisting, indicating a uniform and stable graphene coating on the surface of the constituent fibers (Figure S21).

Figure 5d depicts the EMI shielding efficiency (SE) of different layers of GRAF fabrics in the X-band range (8.2−12.4 GHz). Owing to the electrical insulation of the aramid matrix, the EMI shielding ability of AF was almost negligible.[57,58] The graphene was coated on the surface of the fibers and woven into the fabric, showing an excellent EMI shielding ability. The EMI SE of the material was defined as the logarithmic ratio

https://doi.org/10.1021/acsnano.4c11782
ACS Nano XXXX, XXX, XXX−XXX

between the incoming power (P_i) and transmitted power (P_t) of an electromagnetic wave, expressed in decibels (dB). A higher dB level indicated a lower transmission of electromagnetic waves through the shielding material. For GRAF fabric consisting of a single layer with a thickness of 0.4 mm (the graphene coating content is about 9.85 wt %), the average EMI SE could reach 29.45 dB, effectively blocking 99.874% of incident electromagnetic waves (Figure S22). This meets the commercial requirements for EMI shielding (>20 dB).[59] With an increase in the number of fabric layers, there was a gradual rise in the EMI SE. For the fabric consisting of 5 layers with a thickness of 2 mm, the EMI SE reaches 67.86 dB, effectively blocking 99.999% of incident electromagnetic waves.

To explore the EMI shielding mechanism of GRAF fabrics, the power coefficients A (absorption), R (reflection), and T (transmission) of the fabrics with different layers were calculated according to the scattering parameters.[60] The power coefficient of GRAF fabrics with different numbers of layers exhibited little variation (Figure 5e). Specifically, the R value remained consistently between 0.85 and 0.90, the A value ranged from approximately 0.10 to 0.15, and the T value approached 0. Notably, the R value significantly surpassed both the corresponding A and T values. The coating of the graphene layer optimized the transmission path and movement speed of electrons,[61] resulting in GRAF fabrics with high conductivity to prevent the penetration of electromagnetic waves so that most of the incoming electromagnetic waves were reflected.[62,63] Therefore, the electromagnetic shielding mechanism of GRAF fabrics was dominated by reflection and was supplemented by absorption.

The total EMI effectiveness (SE_T) is the cumulative effect of all attenuating mechanisms, including absorption (SE_A), reflection (SE_R), and multiple reflections (SE_M).[64] In cases where the shielding by absorption (i.e., absorption loss) is greater than 10 dB, most of the rereflected wave will be absorbed within the shield. Thus, SE_M can be ignored.[65,66] Different from the above power coefficients, SE_R, SE_A, and SE_T are determined based on the penetration of electromagnetic waves through the shielding material. Therefore, the contribution of SE_R and SE_A to SE_T is analyzed to further investigate the EMI shielding mechanism inside the GRAF fabrics. It can be seen from Figure 5f that the SE_A value is always higher than the SE_R value, and the contribution of SE_A to SE_T can be calculated to be 66.65%, 76.18%, 81.81%, 85.85%, and 87.86% for the 1, 2, 3, 4, and 5 layered fabrics, respectively. This means that the incoming electromagnetic waves are eventually absorbed by the fabric after many reflections within the GRAF fabric gap. In addition, with the increase of GRAF fabric thickness, the SE_R value has little change, while the SE_A value has a significant increase trend. Therefore, the improved EMI shielding performance of thicker GRAF fabrics can be attributed to the enhanced absorption loss from incoming electromagnetic waves.

To quantitatively compare the EMI shielding properties of GRAF fabrics with those of other previously reported materials, we propose a specific SE value (denoted as SE/content), which represents the ratio of SE to effective shielding substance content. Figure 5g summarizes the SE/content as a function of different EMI shielding material thicknesses including metal-based, MXene-based, CNT-based, and graphene-based materials. Table S3 provides detailed data on SE/content compared to thickness. Although the incorporation of metal as a shielding substance into the composites demonstrated exceptionally high SE values, the high density of the metal additives resulted in a low SE/content value for the composites. The results demonstrate that GRAF fabrics exhibit significantly higher SE/content (298.98 dB) values compared to previously reported shielding materials at a relatively low fabric thickness (0.4 mm) and low graphene coating content (~9.85 wt %). With excellent EMI shielding performance and low shielding substance content, GRAF has great potential for the lightweight composite shielding applications.[67,68]

The EMI shielding mechanism of the fabric is shown in Figure 5h. When an electromagnetic wave radiated to the surface of the GRAF fabric, most of the electromagnetic waves were reflected directly due to the impedance mismatch between the air and the conductive fabric. A minor portion of electromagnetic waves infiltrated into the conductive fabric's surface and interacted with free electrons, resulting in conduction loss.[69] Furthermore, owing to the porous network structure formed during weaving and layer-by-layer self-assembly between the fabrics, multiple reflections occur within this network, thereby elongating the electromagnetic wave transmission path and facilitating further attenuation. Consequently, almost no electromagnetic waves could permeate through the fabrics. It can be concluded that the electromagnetic shielding mechanism of the fabrics is dominated by reflection and assisted by absorption. The effective combination of these two shielding mechanisms determines the final EMI performance of the GRAF fabrics.

CONCLUSIONS

The structural−functional integrated GRAF with both high conductivity and high strength was successfully fabricated through an APA binder-assisted self-assembly strategy. The electrical conductivity of the GRAF is 1062.04 ± 116.78 S/m, while its tensile strength and modulus are 4.66 ± 0.16 GPa and 106.33 ± 8.21 GPa, respectively. These combined properties endow the GRAF fabric with an excellent EMI SE of up to 67.86 dB, along with rapid electrothermal response characteristics. Our findings present innovative approaches for synthesizing structural-functional integrated aramid fibers and fabrics exhibiting exceptional mechanical strength and electrical conductivity.

EXPERIMENTAL SECTION

Materials and Reagents. All chemicals, including dimethylacetamide (DMAc, ≥99%) with water content lower than 50 ppm, lithium chloride (LiCl, >99%), polyvinylpyrrolidone (PVP, K40), terephthaloyl chloride (TPC, >99%), *p*-phenylenediamine (PPD, >99%), 2-(4-aminophenyl)-1*H*-benzimidazol-5-amine (PABZ, ≥99.5%), and potassium hydroxide (KOH, 95%) were purchased from suppliers. The AF was obtained from our group. The raw graphene was procured from Deyang Carbonene Technology Co., Ltd.

In Situ Synthesis of Aramid Polymer Solutions. The monomers *p*-phenylenediamine (3.14 g) and 2-(4-aminophenyl)-5-aminobenzimidazole (9.77 g) were added to a solution of DMAc (500 g)/LiCl (17.5 g) and stirred for 1 h. Subsequently, terephthalate chloride (14.74 g) was introduced into the mixture, and the mixture was stirred for 1.5 h. The resulting aramid polymer solutions demonstrate a dynamic viscosity within the range of 40 000−60 000 mPa·s.

Preparation of APA Dispersion. The prepared aramid polymer solutions (10 g) were mixed with DMAc (190 g), and uniformly diluted aramid polymer solutions were obtained after vigorous stirring for 10 min. Subsequently, KOH (0.6 g) was dissolved in deionized water (8 g) to form KOH aqueous solutions. Finally, the prepared

https://doi.org/10.1021/acsnano.4c11782
ACS Nano XXXX, XXX, XXX−XXX

KOH aqueous solutions were added dropwise into the diluted aramid polymer solutions, and continuous stirring for 30 min was performed to form a deprotonated APA dispersion that can be used for coating. The preparation of APA is carried out in a dry environment at room temperature.

Preparation of Graphene Dispersion. A certain amount of polyvinylpyrrolidone (PVP) was dissolved in DMAc solvent (100 g), followed by the addition of graphene with different weights (0.1, 0.2, and 0.4 g) to the above solution and subsequent ultrasonication for 1 h to achieve uniformly dispersed graphene dispersion. Herein, the weight ratio of PVP to graphene is 2:1. Different concentrations of graphene dispersions (1, 2, and 4 mg/g) can be obtained by adjusting the amount of graphene and PVP added.

Preparation of GRAF, APAF, GKAF, and GAF Fibers. The preparation of GRAF follows the steps below: First, the AF was immersed in APA dispersions for approximately 1 min. This step aims to enhance the adsorption and microetching of APA on the surface of the AF fiber, thereby effectively improving its surface activity and functionalization as a solid foundation for subsequent graphene coating. Second, the treated fiber was submerged directly into the graphene dispersions (2 mg/g) for another 1 min to ensure uniform attachment of graphene onto the fiber's surface. Subsequently, drying the soaked fiber in an oven at 100 °C for 10 min was done to firmly bond and integrate the graphene coating onto the fiber through heat treatment. Finally, the fibers undergo a washing step to remove any surface impurities before being dried (100 °C, 10 min) and rolled into GRAF. In contrast, the preparation process of APAF follows a similar procedure but does not involve graphene coating. The preparation process of GKAF involves the following steps: First, the AF was immersed in KOH aqueous solutions (KOH, 0.6 g; deionized water, 8 g) for 1 min. Subsequently, the aforementioned fibers were soaked in graphene dispersions (concentration, 2 mg/g) for 1 min. Finally, the GKAF was obtained by drying (100 °C, 10 min), washing to remove the impurities on the surface of the fibers, drying (100 °C, 10 min), and rolling. Compared with GKAF, the preparation of GAF does not require KOH etching treatment, and the other processes are completely the same.

ASSOCIATED CONTENT

Supporting Information

The Supporting Information is available free of charge at https://pubs.acs.org/doi/10.1021/acsnano.4c11782.

SEM images, TEM images, Raman spectra, and other graphs and data (PDF)

AUTHOR INFORMATION

Corresponding Authors

Kun Jiao − *School of Materials Science and Engineering, Peking University, Beijing 100871, China; Beijing Graphene Institute (BGI), Beijing 100095, China*; Email: jiaokun-cnc@pku.edu.cn

Xin Gao − *School of Materials Science and Engineering, Peking University, Beijing 100871, China; Beijing Graphene Institute (BGI), Beijing 100095, China*; Email: gaoxin-cnc@pku.edu.cn

Jin Zhang − *School of Materials Science and Engineering, Peking University, Beijing 100871, China; Beijing Graphene Institute (BGI), Beijing 100095, China; College of Chemistry and Molecular Engineering, Peking University, Beijing 100871, China*; orcid.org/0000-0003-3731-8859; Email: jinzhang@pku.edu.cn

Authors

Quanfen Guo − *School of Materials Science and Engineering, Peking University, Beijing 100871, China; Beijing Graphene Institute (BGI), Beijing 100095, China*

Huahui Tian − *Beijing Graphene Institute (BGI), Beijing 100095, China; School of Chemistry and Chemical Engineering, Ningxia University, Yinchuan 750021, China*

Yao Cheng − *Beijing Graphene Institute (BGI), Beijing 100095, China*

Shijun Wang − *National Center for Nanoscience and Technology, Beijing 100190, China*

Zhaolong Li − *Beijing Graphene Institute (BGI), Beijing 100095, China; School of Chemistry and Chemical Engineering, Ningxia University, Yinchuan 750021, China*

He Hao − *College of Chemistry and Molecular Engineering, Peking University, Beijing 100871, China*

Jiayi Liu − *Beijing Graphene Institute (BGI), Beijing 100095, China; Academy for Advanced Interdisciplinary Studies, Peking University, Beijing 100871, China*

Complete contact information is available at: https://pubs.acs.org/10.1021/acsnano.4c11782

Author Contributions

▽These authors contributed equally to this work: Quanfen Guo, Huahui Tian, and Yao Cheng.

Notes

The authors declare no competing financial interest.

ACKNOWLEDGMENTS

This work was financially supported by the National Natural Science Foundation of China (Grants T2188101, 52021006, and 52302034), the Ministry of Science and Technology of China (Grants 2022YFA1203302, 2022YFA1203304, and 2018YFA0703502), the China Postdoctoral Science Foundation (Grant 2022M720205), the Strategic Priority Research Program of CAS (Grant XDB36030100), the Beijing National Laboratory for Molecular Sciences (BNLMS-CXTD-202001), and the Shenzhen Science and Technology Innovation Commission (Grant KQTD20221101115627004). X.G. thanks the Fundamental Research Funds for the Central Universities, Peking University.

REFERENCES

(1) Luo, J.; Wen, Y.; Jia, X.; Lei, X.; Gao, Z.; Jian, M.; Xiao, Z.; Li, L.; Zhang, J.; Li, T.; Dong, H.; Wu, X.; Gao, E.; Jiao, K.; Zhang, J. Fabricating strong and tough aramid fibers by small addition of carbon nanotubes. *Nat. Commun.* **2023**, *14*, 3019.

(2) Penn, L.; Milanovich, F. Raman spectroscopy of Kevlar 49 fibre. *Polymer* **1979**, *20*, 31−36.

(3) Dobb, M.; Johnson, D.; Saville, B. Compressional behaviour of Kevlar fibres. *Polymer* **1981**, *22*, 960−965.

(4) Yan, D.; Luo, J.; Wang, S.; Han, X.; Lei, X.; Jiao, K.; Wu, X.; Qian, L.; Zhang, X.; Zhao, X.; Di, J.; Zhang, Z.; Gao, Z.; Zhang, J. Carbon Nanotube-Directed 7 GPa Heterocyclic Aramid Fiber and Its Application in Artificial Muscles. *Adv. Mater.* **2024**, *36*, 2306129.

(5) Gonzalez, G. M.; Ward, J.; Song, J.; Swana, K.; Fossey, S. A.; Palmer, J. L.; Zhang, F. W.; Lucian, V. M.; Cera, L.; Zimmerman, J. F.; et al. Para-aramid fiber sheets for simultaneous mechanical and thermal protection in extreme environments. *Matter* **2020**, *3*, 742−758.

(6) Wang, H.; Wang, H.; Wang, Y.; Su, X.; Wang, C.; Zhang, M.; Jian, M.; Xia, K.; Liang, X.; Lu, H.; Li, S.; Zhang, Y. Laser Writing of Janus Graphene/Kevlar Textile for Intelligent Protective Clothing. *ACS Nano* **2020**, *14*, 3219−3226.

(7) Lv, J.; Cheng, Z.; Wu, H.; He, T.; Qin, J.; Liu, X. In-situ polymerization and covalent modification on aramid fiber surface via direct fluorination for interfacial enhancement. *Compos. Pt. B-Eng.* **2020**, *182*, 107608.

(8) Cao, C.; Peng, J.; Liang, X.; Saiz, E.; Wolf, S. E.; Wagner, H. D.; Jiang, L.; Cheng, Q. Strong, conductive aramid fiber functionalized by graphene. *Compos. Pt. A-Appl. Sci. Manuf.* **2021**, *140*, 106161.
(9) Zang, H.; Wang, Z.; Qin, S.; Liu, D.; Usman, K.; Razal, J.; Hegh, D.; Lei, W. Multifunctional and ultrastrong MXene modified aramid fibers. *Mater. Today Chem.* **2023**, *33*, 101674.
(10) Little, B. K.; Li, Y.; Cammarata, V.; Broughton, R.; Mills, G. Metallization of Kevlar Fibers with Gold. *ACS Appl. Mater. Interfaces* **2011**, *3*, 1965−1973.
(11) Lee, J.; Kwon, H.; Seo, J.; Shin, S.; Koo, J. H.; Pang, C.; Son, S.; Kim, J. H.; Jang, Y. H.; Kim, D. E.; Lee, T. Conductive Fiber-Based Ultrasensitive Textile Pressure Sensor for Wearable Electronics. *Adv. Mater.* **2015**, *27*, 2433−2439.
(12) Bi, L.; Perry, W.; Wang, R.; Lord, R.; Hryhorchuk, T.; Inman, A.; Gogotsi, O.; Balitskiy, V.; Zahorodna, V.; Baginskiy, I.; Vorotilo, S.; Gogotsi, Y. MXene Functionalized Kevlar Yarn via Automated, Continuous Dip Coating. *Adv. Funct. Mater.* **2024**, *34*, 2312434.
(13) Xie, Y.; Liu, S.; Huang, K.; Chen, B.; Shi, P.; Chen, Z.; Liu, B.; Liu, K.; Wu, Z.; Chen, K.; et al. Ultra-broadband strong electromagnetic interference shielding with ferromagnetic graphene quartz fabric. *Adv. Mater.* **2022**, *34*, 2202982.
(14) Tang, J.; Zhang, X.; Wang, J.; Zou, R.; Wang, L. Achieving flexible and durable electromagnetic interference shielding fabric through lightweight and mechanically strong aramid fiber wrapped in highly conductive multilayer metal. *Appl. Surf. Sci.* **2021**, *565*, 150577.
(15) Fang, H.; Yuan, L.; Liang, G.; Gu, A. Aramid fibre-based wearable electrochemical capacitors with high energy density and mechanical properties through chemical synergistic combination of multi-coatings. *Electrochim. Acta* **2018**, *284*, 149−158.
(16) Gong, X.; Liu, Y.; Wang, Y.; Xie, Z.; Dong, Q.; Dong, M.; Liu, H.; Shao, Q.; Lu, N.; Murugadoss, V.; Ding, T.; Guo, Z. Amino graphene oxide/dopamine modified aramid fibers: Preparation, epoxy nanocomposites and property analysis. *Polymer* **2019**, *168*, 131−137.
(17) Lui, C. H.; Liu, L.; Mak, K. F.; Flynn, G. W.; Heinz, T. F. Ultraflat graphene. *Nature* **2009**, *462*, 339.
(18) Geim, A. K. Graphene: status and prospects. *science* **2009**, *324*, 1530−1534.
(19) Geim, A. K.; Novoselov, K. S. The rise of graphene. *Nat. Mater.* **2007**, *6*, 183−192.
(20) Soldano, C.; Mahmood, A.; Dujardin, E. Production, properties and potential of graphene. *Carbon* **2010**, *48*, 2127−2150.
(21) Fang, B.; Chang, D.; Xu, Z.; Gao, C. A Review on Graphene Fibers: Expectations, Advances, and Prospects. *Adv. Mater.* **2020**, *32*, 1902664.
(22) Wan, S.; Chen, Y.; Fang, S.; Wang, S.; Xu, Z.; Jiang, L.; Baughman, R. H.; Cheng, Q. High-strength scalable graphene sheets by freezing stretch-induced alignment. *Nat. Mater.* **2021**, *20*, 624−631.
(23) Li, X.; Cai, W.; An, J.; Kim, S.; Nah, J.; Yang, D.; Piner, R.; Velamakanni, A.; Jung, I.; Tutuc, E.; et al. Large-area synthesis of high-quality and uniform graphene films on copper foils. *Science* **2009**, *324*, 1312−1314.
(24) Zhang, Z.; Jia, X.; Li, C.; Li, L.; Wen, Y.; Gao, Z.; Zhang, J.; Gao, E.; Jiao, K.; Zhang, J. Simultaneously enhanced interfacial shear strength and tensile strength of heterocyclic aramid fiber by graphene oxide. *Nano Res.* **2023**, *16*, 12286−12293.
(25) Punckt, C.; Muckel, F.; Wolff, S.; Aksay, I. A.; Chavarin, C. A.; Bacher, G.; Mertin, W. The effect of degree of reduction on the electrical properties of functionalized graphene sheets. *Appl. Phys. Lett.* **2013**, *102*, 023114.
(26) Xin, G.; Zhu, W.; Deng, Y.; Cheng, J.; Zhang, L. T.; Chung, A. J.; De, S.; Lian, J. Microfluidics-enabled orientation and microstructure control of macroscopic graphene fibres. *Nat. Nanotechnol.* **2019**, *14*, 168−175.
(27) Wu, S.; Ladani, R. B.; Zhang, J.; Bafekrpour, E.; Ghorbani, K.; Mouritz, A. P.; Kinloch, A. J.; Wang, C. H. Aligning multilayer graphene flakes with an external electric field to improve multifunctional properties of epoxy nanocomposites. *Carbon* **2015**, *94*, 607−618.
(28) Zafar, Z.; Ni, Z. H.; Wu, X.; Shi, Z. X.; Nan, H. Y.; Bai, J.; Sun, L. T. Evolution of Raman spectra in nitrogen doped graphene. *Carbon* **2013**, *61*, 57−62.
(29) Kong, X.; Geng, X.; Geng, S.; Qu, R.; Zhang, Y.; Sun, C.; Wang, J.; Wang, Y.; Ji, C. Antibacterial para-aramid fiber loaded with in situ generated silver nanoparticles. *Surf. Interfaces* **2022**, *30*, 101922.
(30) Li, J.; Wen, Y.; Xiao, Z.; Wang, S.; Zhong, L.; Li, T.; Jiao, K.; Li, L.; Luo, J.; Gao, Z.; Li, S.; Zhang, Z.; Zhang, J. Holey Reduced Graphene Oxide Scaffolded Heterocyclic Aramid Fibers with Enhanced Mechanical Performance. *Adv. Funct. Mater.* **2022**, *32*, 2200937.
(31) Xu, F.; Fan, W.; Zhang, Y.; Gao, Y.; Jia, Z.; Qiu, Y.; Hui, D. Modification of tensile, wear and interfacial properties of Kevlar fibers under cryogenic treatment. *Compos. Pt. B-Eng.* **2017**, *116*, 398−405.
(32) Xu, P.; Yu, Y.; Guo, Z.; Zhang, X.; Li, G.; Yang, X. Evaluation of composite interfacial properties based on carbon fiber surface chemistry and topography: Nanometer-scale wetting analysis using molecular dynamics simulation. *Compos. Sci. Technol.* **2019**, *171*, 252−260.
(33) Lin, J.; Wang, L.; Liu, L.; Lu, K.; Li, G.; Yang, X. Two-stage interface enhancement of aramid fiber composites: Establishment of hierarchical interphase with waterborne polyurethane sizing and oxazolidone-containing epoxy matrix. *Compos. Sci. Technol.* **2020**, *193*, 108114.
(34) Chen, Y.; Ren, J.; Sun, Y.; Liu, W.; Lu, X.; Guan, S. Efficacy of graphene nanosheets on the plasma sprayed hydroxyapatite coating: Improved strength, toughness and in-vitro bioperformance with osteoblast. *Mater. Des.* **2021**, *203*, 109585.
(35) Du, S. S.; Li, F.; Xiao, H. M.; Li, Y. Q.; Hu, N.; Fu, S. Y. Tensile and flexural properties of graphene oxide coated-short glass fiber reinforced polyethersulfone composites. *Compos. Pt. B-Eng.* **2016**, *99*, 407−415.
(36) Kim, K. H.; Oh, Y.; Islam, M. F. Graphene coating makes carbon nanotube aerogels superelastic and resistant to fatigue. *Nat. Nanotechnol.* **2012**, *7*, 562−566.
(37) Li, M.; Zhang, X.; Wang, X.; Ru, Y.; Qiao, J. Ultrastrong graphene-based fibers with increased elongation. *Nano Lett.* **2016**, *16*, 6511−6515.
(38) Zhu, H.; Zhu, S.; Jia, Z.; Parvinian, S.; Li, Y.; Vaaland, O.; Hu, L.; Li, T. Anomalous scaling law of strength and toughness of cellulose nanopaper. *Proc. Natl. Acad. Sci. U.S.A.* **2015**, *112*, 8971−8976.
(39) Lv, J.; Cheng, Z.; Wu, H.; He, T.; Qin, J.; Liu, X. In-situ polymerization and covalent modification on aramid fiber surface via direct fluorination for interfacial enhancement. *Composites, Part B* **2020**, *182*, 107608.
(40) Cao, C.; Peng, J.; Liang, X.; Saiz, E.; Wolf, S. E.; Wagner, H. D.; Jiang, L.; Cheng, Q. Strong, conductive aramid fiber functionalized by graphene. *Compos. Pt. A-Appl. Sci. Manuf.* **2021**, *140*, 106161.
(41) Cheng, B.; Wu, P. Scalable fabrication of kevlar/$Ti_3C_2T_x$ MXene intelligent wearable fabrics with multiple sensory capabilities. *ACS Nano* **2021**, *15*, 8676−8685.
(42) Ma, L.; Nie, Y.; Liu, Y.; Huo, F.; Bai, L.; Li, Q.; Zhang, S. Preparation of Core/Shell Electrically Conductive Fibers by Efficient Coating Carbon Nanotubes on Polyester. *Adv. Fiber Mater.* **2021**, *3*, 180−191.
(43) Deng, H.; Skipa, T.; Bilotti, E.; Zhang, R.; Lellinger, D.; Mezzo, L.; Fu, Q.; Alig, I.; Peijs, T. Preparation of high-performance conductive polymer fibers through morphological control of networks formed by nanofillers. *Adv. Funct. Mater.* **2010**, *20*, 1424−1432.
(44) Zhou, G.; Wang, Y.-Q.; Byun, J.-H.; Yi, J.-W.; Yoon, S.-S.; Cha, H.-J.; Lee, J.-U.; Oh, Y.; Jung, B.-M.; Moon, H.-J.; Chou, T.-W. High-strength single-walled carbon nanotube/permalloy nanoparticle/poly(vinyl alcohol) multifunctional nanocomposite fiber. *ACS Nano* **2015**, *9*, 11414−11421.
(45) Eom, J.; Jaisutti, R.; Lee, H.; Lee, W.; Heo, J. S.; Lee, J. Y.; Park, S. K.; Kim, Y. H. Highly Sensitive Textile Strain Sensors and Wireless User-Interface Devices Using All-Polymeric Conducting Fibers. *ACS Appl. Mater. Interfaces* **2017**, *9*, 10190−10197.

https://doi.org/10.1021/acsnano.4c11782
ACS Nano XXXX, XXX, XXX−XXX

(46) Zeng, J.; Ma, W.; Wang, Q.; Yu, S.; Innocent, M. T.; Xiang, H.; Zhu, M. Strong, high stretchable and ultrasensitive SEBS/CNTs hybrid fiber for high-performance strain sensor. *Compos. Commun.* **2021**, *25*, 100735.
(47) Yu, W.; Li, Y.; Xin, B.; Lu, Z. MXene/PVA fiber-based supercapacitor with stretchability for wearable energy storage. *Fiber Polym.* **2022**, *23*, 2994−3001.
(48) He, Z.; Zhou, G.; Byun, J.-H.; Lee, S.-K.; Um, M.-K.; Park, B.; Kim, T.; Lee, S. B.; Chou, T.-W. Highly stretchable multi-walled carbon nanotube/thermoplastic polyurethane composite fibers for ultrasensitive, wearable strain sensors. *Nanoscale* **2019**, *11*, 5884−5890.
(49) Feng, W.; Zou, L.; Lan, C.; E, S.; Pu, X. Core-Sheath CNT@MXene Fibers Toward Absorption-Dominated Electromagnetic Interference Shielding Fabrics. *Adv. Fiber Mater.* **2024**, *6*, 1657−1668.
(50) Liu, W.; Xue, C.; Long, X.; Ren, Y.; Chen, Z.; Zhang, W. Highly flexible and multifunctional CNTs/TPU fiber strain sensor formed in one-step via wet spinning. *J. Alloys Compd.* **2023**, *948*, 169641.
(51) Yang, L.; Lin, F.; Zabihi, F.; Yang, S.; Zhu, M. High specific capacitance cotton fiber electrode enhanced with PPy and MXene by in situ hybrid polymerization. *Int. J. Biol. Macromol.* **2021**, *181*, 1063−1071.
(52) Cao, C.; Lin, Z.; Liu, X.; Jia, Y.; Saiz, E.; Wolf, S. E.; Wagner, H. D.; Jiang, L.; Cheng, Q. Strong Reduced Graphene Oxide Coated Bombyx mori Silk. *Adv. Funct. Mater.* **2021**, *31*, 2102923.
(53) Ryan, J. D.; Mengistie, D. A.; Gabrielsson, R.; Lund, A.; Müller, C. Machine-Washable PEDOT:PSS Dyed Silk Yarns for Electronic Textiles. *ACS Appl. Mater. Interfaces* **2017**, *9*, 9045−9050.
(54) He, D.; Fan, B.; Zhao, H.; Lu, X.; Yang, M.; Liu, Y.; Bai, J. Design of electrically conductive structural composites by modulating aligned CVD-grown carbon nanotube length on glass fibers. *ACS Appl. Mater. Interfaces* **2017**, *9*, 2948−2958.
(55) Cui, G.; Cheng, Y.; Liu, C.; Huang, K.; Li, J.; Wang, P.; Duan, X.; Chen, K.; Liu, K.; Liu, Z. Massive Growth of Graphene Quartz Fiber as a Multifunctional Electrode. *ACS Nano* **2020**, *14*, 5938−5945.
(56) Wang, Q. W.; Zhang, H. B.; Liu, J.; Zhao, S.; Xie, X.; Liu, L.; Yang, R.; Koratkar, N.; Yu, Z. Z. Multifunctional and Water-Resistant MXene-Decorated Polyester Textiles with Outstanding Electromagnetic Interference Shielding and Joule Heating Performances. *Adv. Funct. Mater.* **2019**, *29*, 1806819.
(57) Zhang, Z.; Wang, C.; Luo, Y.; Yuan, C.; Hu, W. Customize Aramid Nanofiber Aerogels with High Electromagnetic Shielding Performance from Ultra-Malleable Kevlar-Derived Jelly. *Adv. Mater. Technol.* **2023**, *8*, 2300548.
(58) Lu, Z.; Jia, F.; Zhuo, L.; Ning, D.; Gao, K.; Xie, F. Microporous MXene/Aramid nanofibers hybrid aerogel with reversible compression and efficient EMI shielding performance. *Compos. Pt. B-Eng.* **2021**, *217*, 108853.
(59) Chen, Z.; Xu, C.; Ma, C.; Ren, W.; Cheng, H. M. Lightweight and Flexible Graphene Foam Composites for High-Performance Electromagnetic Interference Shielding. *Adv. Mater.* **2013**, *25*, 1296−1300.
(60) Ganguly, S.; Das, P.; Saha, A.; Noked, M.; Gedanken, A.; Margel, S. Mussel-inspired polynorepinephrine/MXene-based magnetic nanohybrid for electromagnetic interference shielding in X-band and strain-sensing performance. *Langmuir* **2022**, *38*, 3936.
(61) Ganguly, S.; Kanovsky, N.; Das, P.; Gedanken, A.; Margel, S. Photopolymerized thin coating of polypyrrole/graphene nanofiber/iron oxide onto nonpolar plastic for flexible electromagnetic radiation shielding, strain sensing, and non-contact heating applications. *Adv. Mater. Interfaces* **2021**, *8*, 2101255.
(62) Chen, W.; Liu, L. X.; Zhang, H. B.; Yu, Z. Z. Flexible, Transparent, and Conductive $Ti_3C_2T_x$ MXene-Silver Nanowire Films with Smart Acoustic Sensitivity for High-Performance Electromagnetic Interference Shielding. *ACS Nano* **2020**, *14*, 16643−16653.
(63) Cheng, M.; Ying, M.; Zhao, R.; Ji, L.; Li, H.; Liu, X.; Zhang, J.; Li, Y.; Dong, X.; Zhang, X. Transparent and Flexible Electromagnetic Interference Shielding Materials by Constructing Sandwich AgNW@MXene/Wood Composites. *ACS Nano* **2022**, *16*, 16996−17007.
(64) Das, P.; Ganguly, S.; Perelshtein, I.; Margel, S.; Gedanken, A. Acoustic green synthesis of graphene-gallium nanoparticles and PEDOT: PSS hybrid coating for textile to mitigate electromagnetic radiation pollution. *ACS Appl. Nano Mater.* **2022**, *5*, 1644−1655.
(65) Sood, Y.; Mudila, H.; Chamoli, P.; Saini, P.; Kumar, A. Exploring the efficacy and future potential of polypyrrole/metal oxide nanocomposites for electromagnetic interference shielding: a review. *Mate. Horiz.* **2024**, *11*, 4256−4274.
(66) Hou, X.; Feng, X. R.; Jiang, K.; Zheng, Y. C.; Liu, J. T.; Wang, M. Recent progress in smart electromagnetic interference shielding materials. *J. Mater. Sci. Technol.* **2024**, *186*, 256−271.
(67) Kong, L.; Yin, X.; Xu, H.; Yuan, X.; Wang, T.; Xu, Z.; Huang, J.; Yang, R.; Fan, H. Powerful absorbing and lightweight electromagnetic shielding CNTs/RGO composite. *Carbon* **2019**, *145*, 61−66.
(68) Zeng, Z.; Jin, H.; Chen, M.; Li, W.; Zhou, L.; Zhang, Z. Lightweight and anisotropic porous MWCNT/WPU composites for ultrahigh performance electromagnetic interference shielding. *Adv. Funct. Mater.* **2016**, *26*, 303−310.
(69) Lee, J.; Liu, Y.; Liu, Y.; Park, S. J.; Park, M.; Kim, H. Y. Ultrahigh electromagnetic interference shielding performance of lightweight, flexible, and highly conductive copper-clad carbon fiber nonwoven fabrics. *J. Mater. Chem. C* **2017**, *5*, 7853−7861.

https://doi.org/10.1021/acsnano.4c11782
ACS Nano XXXX, XXX, XXX−XXX